Quality assessment of reconstruction and relighting from RTI images: application to manufactured surfaces

Abir Zendagui, Jean-Baptiste Thomas, Gaetan Le Goic, Yuly Castro, Marvin Nurit, Alamin Mansouri, Marius Pedersen

Quality assessment of reconstruction and relighting from RTI images: application to manufactured surfaces

Abir Zendagui[1], Jean-Baptiste Thomas[2], Gaëtan Le Goïc [1], Yuly Castro[1],
Marvin Nurit[1],Alamin Mansouri [1], Marius Pedersen[2]
[1]Imagerie et Vision Artificielle Laboratory, UFR Sciences et Techniques University of Burgundy, Dijon, France.
[2] The Norwegian Colour and Visual Computing Laboratory, Department of computer science, NTNU, Gjøvik, Norway
Email: {abir_zendagui, yuly-emilia_castro-cartagena, marvin_nurit}@etu.u-bourgogne.fr
{gaetan.le-goic, alamin.mansouri}@u-bourgogne.fr
{jean.b.thomas, marius.pedersen}@ntnu.no

***Abstract*—In this paper, we propose to evaluate the quality of the reconstruction and relighting, from images acquired by Reflectance Transformation Imaging (RTI) device, of three largely used state-of-art methods, namely PTM, HSH and DMD. We evaluate these methods with regards to an objective evaluation using PSNR and SSIM as well as visual assessment through a sensory (visual) assessment, which is still today the reference in the industry. The evaluation was also carried out with regards to different sampling densities. This study allows to estimate the efficiency of these models to reproduce the aspect of the manufactured surfaces with relevant input parameters for the RTI approach. It also shows that DMD reproduces the most accurate reconstruction/relighting to an acquired measurement and that a higher sampling density don't mean necessarily a higher perceptual quality.**

***Index Terms*—Reflectance Transformation Imaging, psychometric evaluation, relighting.**

I. Introduction

The inspection of manufactured surfaces is generally a visuo-tactile process realized by human experts. It typically consists in changing the product surface orientation to change the light incidence angle, which seems to be the most influential parameter. To ensure the reproducibility and to reduce the variability of results and decisions to make [1] [2], the inspection process has to be automatised or at least semi-automatised (at least light source could be changed automatically). In this sense, the Reflectance Transforming Imaging (RTI) approach seems to be a very adequate technique to automatise and make this Non Destructive Inspection (NDI). It simplifies the inspection conditions since only light position changing is to be considered. This technique is widely used for image relighting, i.e. for reconstructing a scene under an arbitrary (virtual) direction of illumination with applications in Video-games, Cultural heritage and recently in manufacturing.

Agence Nationale de la Recherche through SUMUM and NAPS projects, The Norwegian Colour and Visual Computing Laboratory - NTNU

RTI acquisition process consists in taking a set of images with a fixed camera, orthogonal to the inspected surface, while varying the light direction at each image capture. From this set of images, each pixel is described by a set of discrete values (measured gray-levels, which are considered to be proportional to the luminance [3]). To model the surface visual appearance continuously (corresponds also to relighting), these discrete values can be approximated (for each pixel) by projecting the vector containing the discrete measured gray-levels on a set of basis functions. The main methods used to model this information are Polynomial Texture Mappings (PTM, based on 2nd order polynomial functions)[4], Hemispherical Harmonics (HSH)[5] and a more recent method named Discrete Modal Decomposition (DMD) [6].

In this study, we investigates the accuracy of the reconstruction/relighting from RTI-base images using the three models: PTM, HSH, DMD objectively using the Peak Signal to Noise Ratio (PSNR) and Structural Similarity error metric (SSIM) [7] and subjectively using a psychometric experiment for comparing models with different density of sampling in order to choose the best configuration of parameters to reproduce a perceptual aspect of physical manufactured surfaces.

II. Background

RTI consists in acquiring photometric stereo images corresponding to varying light positions in two directions (elevation and azimuth) with a sensor positioned orthogonal to the surface. According to Durou et al. to [8], the luminance of a pixel is proportional to the grey intensity of the pixel and the formula is written in equation 1

$$G = k * L(U_c) \tag{1}$$

Where **k** is the proportionality factor. **L(U_c)** is the luminance in sensor's direction.

The result of a RTI acquisition is, for each pixel, a vector containing the luminance values corresponding to the different

light positions used during the acquisition stage. To be able to relight a scene under any arbitrary direction an approximation (reconstruction) operation is necessary to build a continuous surface from the sparse point cloud (lunimance values). In the literature, three approximation models are mainly used to achieve this reconstruction: the Polynomial Texture Mapping (PTM), the Hemispherical Harmonics (HSH) based decompostion and the Discrete Modal Decomposition (DMD).

A. Polynomial Texture Mapping (PTM)

The Polynomial Texture Mapping was developed initially to improve the photo-realistic rendering in 3D imaging[4]. Widely used in the cultural heritage [9], PTM approximate the the luminance surface in each pixel by a polynomial regression of 6 vectors $(a_0 - a_5)$. These 6 vectors are sought for each pixel from the quadratic surface representing the reflectance defined by the second degree polynomial equation below:

$$L(l_u, l_v) = a_0 + a_1 l_u + a_2 lv + a_3 l_u l_v + a_4 l_u^2 + a_5 l_v \quad (2)$$

The equation (2) is solved by a regression using the least squares formulation. The PTM's description of the surface is thus still simple and very smooth (no sharp frequency), but it demonstrates its efficiency with a small stack of images to correctly relight the surfaces, especially lambertian ones.

B. Hemispherical Harmonics (HSH)

The Hemispherical Harmonics is an improvement of the PTM technique [10] that implements more complex basis functions [11], [12], [13], [14]derived from Hemispherical harmonics. Gautron et al. defined the hemispheric harmonic bases $H_l^m(\theta, \phi)$ as an adapted version of spherical harmonies $S_l^m(\theta, \phi)$ that rely on derivation of Legendre polynomials (3).

$$P_l^m(cos\theta) = P_l^m(2cos\theta - 1) \; and \; \theta \in \left[0, \frac{\pi}{2}\right] \quad (3)$$

C. Discrete Modal Decomposition (DMD)

The Discrete Modal Decomposition is a technique initially used in dynamic mechanics to decompose a vibration, for the geometrical tolerancing [15] [16], multi-scale analysis of topographic surface roughness[17] [18] [19] and for heat source evaluation [20] [21]. This method was then applied in the field of surface appearance, to model the local behaviour of the reflectance angular component, at each point/pixel. The DMD technique consists in decomposing the signal which represent the measured surface into a family of functions (eigen-modes) resulting from the vibration of basis forms (planar, cylindrical, spherical...) and forming the eigen-basis. The eigen-basis is defined by eigen-vectors called Modal vectors. The modal bases derives from the resolution of the classical dynamic equation (4).

$$K.q + M.\ddot{q} = 0 \quad (4)$$

With

$$q = q(x, y, t) = \sum_{i=1}^{+\infty} Q_i(x, y).cos(\omega_i t) \quad (5)$$

Where M is Mass matrix, K is the stiffness matrix and $q(x, y, t)$ is the displacements that characterizes the modal shapes. The projection of the measured surface onto the modal basis is then the sum of a linear combination of modal vectors and the decomposition residual (6)

$$V = \sum_{i=1}^{N_q} \lambda_i Q_i + \epsilon(N_q) \quad (6)$$

With Q_i is the modal vectors composing the modal basis. λ_i is the modal coordinates and N_q is the number of modes of decomposition.

In Figure 1, reconstruction results for the same pixel using the three approximations PTM, HSH and DMD are presented.

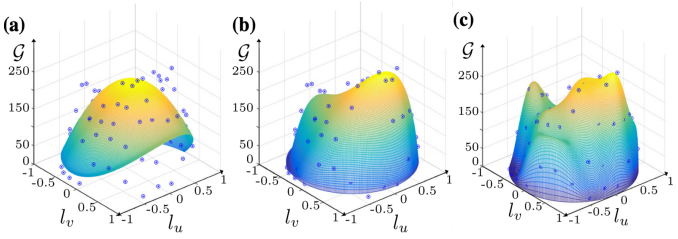

Fig. 1. Reconstruction of the same pixel using, from left to right, using PTM, HSH and DMD modeling

III. Proposed Evaluation

A. Dataset

1) Acquisition device: The RTI acquisition device we used in this study is a home-made one built in a manner to be able to position the light source precisely for any couple θ and ϕ since the light source is fixed on a rotated hoop. This configuration allows to construct a virtual lightening dome around the surface with flexible positioning of the light source. The camera and the lenses were chosen to ensure high quality and high resolution images.

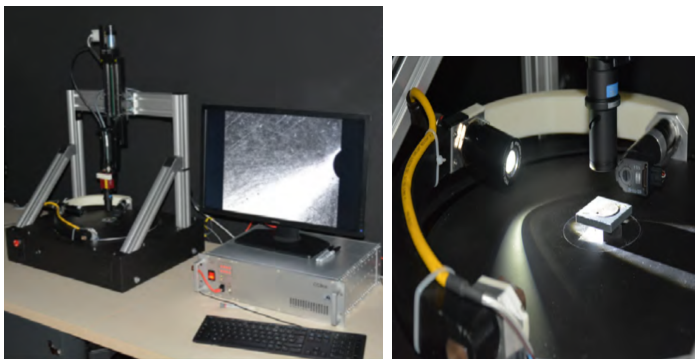

Fig. 2. Home-made x-RTI system for surface appearance acquisition.

2) Samples: The manufactured surfaces used in this study are ten metallic sides of manufactured rings. These surfaces, called LGR, were polished and finished with a tribofinition process, composed of three main successive treatments: Softening, polishing, brightening. The ten rings are grouped two by two in five process groups. The only difference between groups is the time that surfaces passed in the softening step and it is varying from 40 minutes and 80 minutes which makes the rugosity varying from $0.22\mu m$ to $0.17\mu m$.

3) Data preparation: To build our dataset for the experiment, a dense (650 measurements: 130 in θ and 5 in ϕ) photometric stereo acquisition was taken with the system described previously for three plane sides of the ten rings presented in section III-A2. For each model the contributions are calculated with 6 terms for PTM, 9 harmonies for HSH and 50 modes for DMD. To estimate the visual quality of the RTI-based reconstructions, the direction of the virtual lighting used is the same for the measured image, see example in Figure 4. Five perpendicular to the surface light directions were chosen: $(\theta : 180°, \phi : 14.5°), (\theta : 180°, \phi : 28°), (\theta : 180°, \phi : 41.5°), (\theta : 180°, \phi : 55°), (\theta : 180°, \phi : 14.5°), (\theta : 88.6154°, \phi : 41.5°)$

Fig. 3. Manufactured rings

B. Objective evaluation

The first metric we used for the objective evaluation is the Peak Signal to Noise Ratio (PSNR) since it has already proven its relevance in RTI data. For instance, it has already been used to evaluate the efficiency of the fitting models reproductions [22] [23], to evaluate the RTI compressed images quality to be visualised on a mobile device [24] or on a web pages [25]. This pixel-to-pixel quality metric is used in this study in perspective to correlate it with subjective experiment and to continue the investigation on the perceptual quality of the fitting models in [22]. In Table II, the peak signal-to-noise ratio for the reproduced image using the three approximation models with the reference (captured photos). For each sampling density (All, Half, Fifth, Seventh), the images were reproduced in 5 light directions to study the impact of the exposure of the surface to the light on the reproduced image. In Table III the PSNR is computed over the 5 surfaces corresponding to the 5 fabrication process, using the DMD with the chosen sampling densities.

In a second step for the objective evaluation, we added a new metric namely Structural Similarity (SSIM) index, which seems to take more in consideration the spatial aspect and consequently the human visual perception. This metric uses in its computation three terms: luminance, the contrast, and structural term [7]. Same for PSNR, we computed the structural similarity in Table VII of the reproduced images using the three approximation models in different sampling density (All, Half, Fifth, Seventh) in 5 light directions. In Table VIII the SSIM is computed only using DMD with different density sampling for the 5 used surfaces in the study. Each surface were token from a different group process to investigate on future studies the impact of the fabrication process on the evaluation of the surfaces. In order to see the mean and the median ranking of models, the Table V were computed to see the behaviour of the quality of the reproductions over the approximation models, and over sampling densities in the Table VI.

C. results and discussion

We notice in Table I that the global mean and medium of PSNR can rank easily the reproduced images quality as PTM, HSH, DMD respectively from the worst to the best. This rank is less obvious with 1/7 sampling density between HSH and DMD using PSNR in Table II where HSH and DMD are having respectively 30.78 and 30.37 in $(\theta : 180°, \phi : 14.5°)$ and 25.83, 25.89 in $(\theta : 180°, \phi : 28°)$ and 23.29, 23.20 in $(\theta : 88.61°, \phi : 41.5°)$. The same results for SSIM in Table VII were the difference between the models is reduced using 1/7 of the measurements (93 image) to at least 0.03. Regarding the quality of reproductions using DMD over the 5 manufactured surfaces in Table III using PSNR and in Table VIII using SSIM, a higher scores where for 1/5 of measurements in two angles $(\theta : 180°, \phi : 28°)$ and $(\theta : 180°, \phi : 55°)$ for all the surfaces which mean a higher quality of reproduction with this sampling density in this two angles comparing to the captured image. For the angle $(\theta : 180°, \phi : 41.5°)$ in Table VIII the 1/2 sampling density where more accurate to the captured image using SSIM and PSNR for the five surfaces.

TABLE I
GLOBAL MEAN AND MEDIAN OF PSNR COMPUTED OVER 5 REPRODUCED SURFACES' ASPECT THE 5 LIGHT DIRECTIONS

Method	Mean	Median
PTM	17.46	19.46
HSH	24.52	23.47
DMD	26.76	25.67

Despite the results of PSNR and SSIM that DMD outperforms the other models and some other conclusions that we can make considering these results, it's important to mention that these error metrics are a pixel to pixel comparisons and no consideration to the biological human vision system, for that reason a further psychometric experiment were done to evaluate subjectively the perceived quality of the reproductions using RTI protocol.

TABLE II
PEAK SIGNAL-TO-NOISE RATIO FOR THE REPRODUCED IMAGES USING PTM, HSH, DMD AND 4 SAMPLING DENSITY (ALL, HALF, FIFTH AND SEVENTH) WITH THE ACQUIRED IMAGES IN DIFFERENT ANGLES.

Sampling	Angle	PTM	HSH	DMD
All (1): 650 position	$\theta : 180°, \phi : 14.5°$	12,13	31,06	34,87
	$\theta : 180°, \phi : 28°$	20,65	26,17	29,11
	$\theta : 180°, \phi : 41.5°$	19,46	22,64	25,43
	$\theta : 180°, \phi : 55°$	14,90	19,52	22,37
	$\theta : 88.61°, \phi : 41.5°$	20,26	23,60	26,06
Half (1/2): 324 position	$\theta : 180°, \phi : 14.5°$	12,10	31,03	34,84
	$\theta : 180°, \phi : 28°$	20,66	26,17	28,83
	$\theta : 180°, \phi : 41.5°$	19,47	22,66	25,53
	$\theta : 180°, \phi : 55°$	14,87	19,51	22,23
	$\theta : 88.61°, \phi : 41.5°$	20,26	23,57	25,82
Fifth (1/5): 130 position	$\theta : 180°, \phi : 14.5°$	12,09	30,91	33,62
	$\theta : 180°, \phi : 28°$	20,66	26,28	30,14
	$\theta : 180°, \phi : 41.5°$	19,47	22,63	24,69
	$\theta : 180°, \phi : 55°$	14,89	19,60	22,99
	$\theta : 88.61°, \phi : 41.5°$	20,25	23,37	24,21
Seventh (1/7): 93 position	$\theta : 180°, \phi : 14.5°$	12,10	**30,78**	**30,37**
	$\theta : 180°, \phi : 28°$	20,59	**25,83**	**25,89**
	$\theta : 180°, \phi : 41.5°$	19,42	22,50	24,42
	$\theta : 180°, \phi : 55°$	14,80	19,31	20,60
	$\theta : 88.61°, \phi : 41.5°$	20,25	**23,29**	**23,20**

TABLE III
PEAK SIGNAL-TO-NOISE RATIO FOR THE REPRODUCED IMAGES USING DMD AND 4 SAMPLING DENSITY (ALL, HALF, FIFTH AND SEVENTH) WITH THE ACQUIRED IMAGES IN DIFFERENT ANGLES FOR THE FIVE MANUFACTURED SURFACES

Surfaces	Angles	ALL	HALF	FIFTH	SEVEN
Surface 1:A01	$(180°, 14.5°)$	34,87	34,84	33,62	30,37
	$(180°, 28°)$	29,11	28,83	**30,14**	25,89
	$(180°, 41.5°)$	25,43	25,53	**24,69**	24,42
	$(180°, 55°)$	22,37	22,23	**22,99**	20,60
	$(88.61°, 41.5°)$	26,06	25,82	24,21	23,20
Surface 2: A04	$(180°, 14.5°)$	36,10	36,05	34,80	31,52
	$(180°, 28°)$	31,14	30,84	**32,26**	27,92
	$(180°, 41.5°)$	27,29	**27,38**	26,76	26,30
	$(180°, 55°)$	23,75	23,61	**24,55**	21,69
	$(88.61°, 41.5°)$	24,71	24,48	22,81	21,86
Surface 3: A06	$(180°, 14.5°)$	35,21	35,15	34,09	30,90
	$(180°, 28°)$	30,64	30,39	**31,45**	27,26
	$(180°, 41.5°)$	27,96	**28,04**	27,14	26,93
	$(180°, 55°)$	24,74	24,59	**25,35**	22,63
	$(88.61°, 41.5°)$	23,56	23,30	21,73	20,65
Surface 4: A07	$(180°, 14.5°)$	36,37	36,31	35,15	31,55
	$(180°, 28°)$	30,32	29,98	**31,61**	27,40
	$(180°, 41.5°)$	26,76	**26,88**	26,17	25,85
	$(180°, 55°)$	23,59	23,41	**24,48**	21,60
	$(88.61°, 41.5°)$	26,01	25,68	24,17	23,17
Surface 5: A10	$(180°, 14.5°)$	37,20	37,16	35,83	32,63
	$(180°, 28°)$	31,88	31,47	**32,58**	28,51
	$(180°, 41.5°)$	27,49	**27,60**	26,50	26,00
	$(180°, 55°)$	23,35	23,14	**23,98**	21,53
	$(88.61°, 41.5°)$	26,58	26,28	24,86	23,94

TABLE IV
GLOBAL MEAN AND MEDIAN OF PSNR COMPUTED OVER 5 REPRODUCED SURFACES' ASPECT IN 5 LIGHT DIRECTIONS USING ALL/HALF/FIFTH/SEVENTH OF MEASUREMENTS

Method	ALL	HALF	FIFTH	SEVENTH
Mean	28.29	28.16	27.86	25.57
Median	27.02	27.13	26.33	25.82

TABLE V
GLOBAL MEAN AND MEDIAN OF SSIM COMPUTED OVER 5 REPRODUCED SURFACES' ASPECT IN 5 LIGHT DIRECTIONS

Method	Mean	Median
PTM	0.37	0.42
HSH	0.65	0.67
DMD	0.73	0.73

TABLE VI
GLOBAL MEAN AND MEDIAN OF SSIM COMPUTED OVER 5 REPRODUCED SURFACES' ASPECT IN 5 LIGHT DIRECTIONS USING ALL/HALF/FIFTH/SEVENTH OF MEASUREMENTS

Method	ALL	HALF	FIFTH	SEVENTH
Mean	0.77	0.76	0.74	0.64
Median	0.76	0.77	0.72	0.68

D. Visual assessment

To evaluate the performance of the reconstruction (fitting) models (PTM, HSH, DMD) to reproduce the visual aspect of the manufactured surfaces used in the study, a psychometric experiment was designed in two parts to answer two main goals:

- The impact of the fitting models on the reproduction of the aspect of manufactured surfaces.
- The impact of the sampling density to approximate perceptual aspect of surfaces.

1) Controlled psychometric experiment: The psychometric experiment were carried out on a dedicated web-based platform for psychometric scaling experiments: QuickEval[26]. In order to increase the perceived contrast of images with the environment, a black background was picked-out for the webpage and the experiment held in a dark room (no lighting

TABLE VII
STRUCTURAL SIMILARITY FOR THE REPRODUCED IMAGES USING PTM, HSH, DMD AND 4 SAMPLING DENSITY (ALL, HALF, FIFTH AND SEVENTH) WITH THE ACQUIRED IMAGES IN DIFFERENT ANGLES.

Sampling	Angle	PTM	HSH	DMD
All (1): 650 position	$\theta : 180°, \phi : 14.5°$	0,17	0,70	0,88
	$\theta : 180°, \phi : 28°$	0,42	0,71	0,83
	$\theta : 180°, \phi : 41.5°$	0,49	0,68	0,76
	$\theta : 180°, \phi : 55°$	0,34	0,54	0,66
	$\theta : 88.61°, \phi : 41.5°$	0,46	0,66	0,75
Half (1/2): 324 position	$\theta : 180°, \phi : 14.5°$	0,17	0,70	0,88
	$\theta : 180°, \phi : 28°$	0,42	0,71	0,82
	$\theta : 180°, \phi : 41.5°$	0,49	0,68	0,77
	$\theta : 180°, \phi : 55°$	0,33	0,54	0,64
	$\theta : 88.61°, \phi : 41.5°$	0,46	0,65	0,73
Fifth (1/5): 130 position	$\theta : 180°, \phi : 14.5°$	0,17	0,69	0,84
	$\theta : 180°, \phi : 28°$	0,42	0,71	0,84
	$\theta : 180°, \phi : 41.5°$	0,48	0,66	0,70
	$\theta : 180°, \phi : 55°$	0,33	0,56	0,72
	$\theta : 88.61°, \phi : 41.5°$	0,45	0,63	0,64
Seventh (1/7): 93 position	$\theta : 180°, \phi : 14.5°$	0,16	0,69	0,74
	$\theta : 180°, \phi : 28°$	0,41	**0,68**	**0,69**
	$\theta : 180°, \phi : 41.5°$	0,48	**0,66**	**0,69**
	$\theta : 180°, \phi : 55°$	0,31	**0,50**	**0,51**
	$\theta : 88.61°, \phi : 41.5°$	0,45	**0,62**	**0,59**

TABLE VIII
STRUCTURAL SIMILARITY FOR THE REPRODUCED IMAGES USING DMD AND 4 SAMPLING DENSITY (ALL, HALF, FIFTH AND SEVENTH) WITH THE ACQUIRED IMAGES IN DIFFERENT ANGLES FOR THE FIVE SURFACES.

Surfaces	Angles	ALL	HALF	FIFTH	SEVEN
Surface 1:A01	$(180°, 14.5°)$	0,88	0,88	0,84	0,74
	$(180°, 28°)$	0,83	0,82	**0,84**	0,69
	$(180°, 41.5°)$	0,76	**0,77**	0,70	0,69
	$(180°, 55°)$	0,66	0,64	**0,72**	0,51
	$(88.61°, 41.5°)$	0,75	0,73	0,64	0,59
Surface 2: A04	$(180°, 14.5°)$	0,88	0,88	0,84	0,74
	$(180°, 28°)$	0,84	0,82	**0,86**	0,70
	$(180°, 41.5°)$	0,76	**0,77**	0,71	0,69
	$(180°, 55°)$	0,65	0,63	**0,72**	0,49
	$(88.61°, 41.5°)$	0,69	0,66	0,56	0,50
Surface 3: A06	$\theta : 180°, 14.5°)$	0,84	0,84	0,80	0,72
	$(180°, 28°)$	0,84	0,82	**0,84**	0,70
	$(180°, 41.5°)$	0,79	**0,80**	0,73	0,71
	$(180°, 55°)$	0,68	0,66	**0,73**	0,53
	$(88.61°, 41.5°)$	0,68	0,65	0,56	0,50
Surface 4: A07	$(180°, 14.5°)$	0,90	0,89	0,85	0,76
	$(180°, 28°)$	0,85	0,83	**0,86**	0,71
	$(180°, 41.5°)$	0,75	**0,76**	0,69	0,67
	$(180°, 55°)$	0,64	0,61	**0,72**	0,48
	$(88.61°, 41.5°)$	0,71	0,67	0,58	0,53
Surface 5: A10	$(180°, 14.5°)$	0,91	0,90	0,87	0,79
	$(180°, 28°)$	0,86	0,84	**0,87**	0,73
	$(180°, 41.5°)$	0,76	**0,77**	0,69	0,66
	$(180°, 55°)$	0,63	0,59	**0,71**	0,47
	$(88.61°, 41.5°)$	0,76	0,73	0,66	0,62

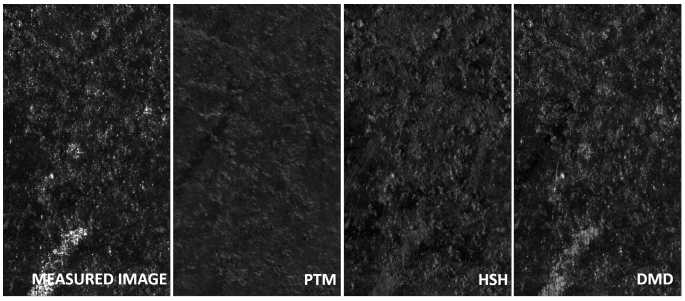

Fig. 4. Example of a measured image with RTI-based reconstructions in same lighting direction $(\theta : 180°, \phi : 41.5°)$

with matt grey wall). The experiment is a paired comparison [27] where participants' task is to choose the most similar representation (the reconstructed images using two of the three fitting models each time, positioned on the left and on the right) to the original image (the acquired image positioned in the middle). The experiment was setup as a forced-choice experiment with flipping of the pairs. The experiment divided on two parts took in average 30 minutes (10 minutes for the 1^{st} part and 20 minutes for the 2^{nd} part) for 240 comparison in total. The two parts answer respectively to the main goals presented in section III-D.

2) Participants: The participants involved in this experiment were 19 volunteer researchers working at the Norwegian Colour and Visual Computing Laboratory. They can be considered as experienced observers in psychometric experiments.

3) Results and discussion: In Figure 6, a comparison of users' preferences comparing the three approximation models using all the measurements (All the acquired Images to approximate the visual aspect) of the acquisition. The five groups of the graph are according to the chosen five angles for the experiment and as shown, more than 60% of users picked out DMD as the more accurate reproduction to the reference shown (raw image). Roughly 30% of them chose HSH which is a good evaluation of the quality of images using this model, but we believe that this amount of votes is due to the cases were the user had to choose between HSH and PTM, this latter is a model rarely chosen for the quality of reconstructed images. Only 6% of user's preferences were for PTM in $(\theta : 180°, \phi : 14.5°)$ using all the measurements and 1% using one seventh of measurement in the same angle and 0% in $(\theta : 180°, \phi : 55°)$ and this is due to poorness of PTM to approximate the luminance of the pixel defined by a quadratic surface (simple geometry) and which average the pixel's luminance under exposed $(\theta : 180°, \phi : 14.5°)$ and overexposed $(\theta : 180°, \phi : 55°)$ to the light. In $(\theta : 88.6154°, \phi : 41.5°)$ PTM do a better in Table 7, comparing to its performance in the other cases, the reason is that PTM's regression formulation (Least squares) is more efficient with less information : minimum residual.

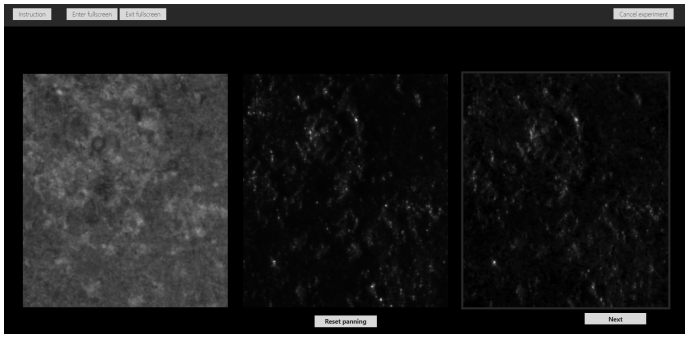

Fig. 5. Screen shot of one example of the proposed experiment in QuiqEval platform, in the center the original image, in left and right two reproduced images using two of the three approximation models

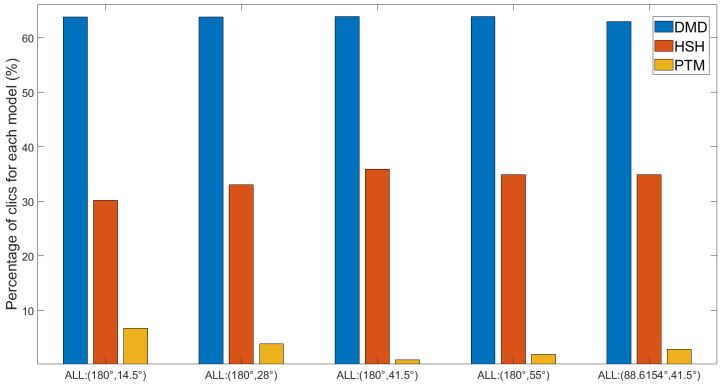

Fig. 6. Number of times a reproduction has been selected using the three fitting models : DMD, HSH, PTM using all the measurements

These results are detailed and extended in Table IX for all the angles and sampling density used in the study, where the

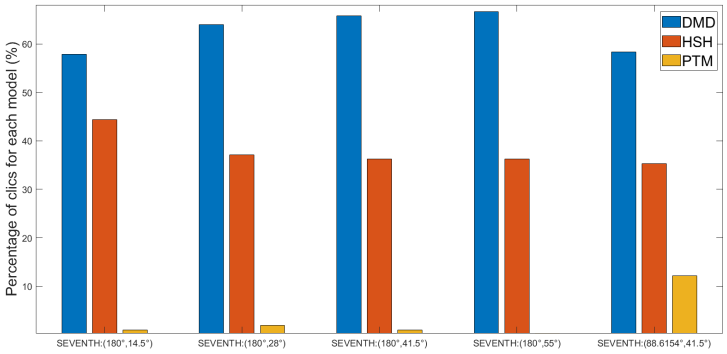

Fig. 7. Number of times a reproduction has been selected using the three fitting models : DMD, HSH, PTM using 1/7 of the measurements

standard deviation to the mean is ~ 2 for DMD in 15/20 of cases which makes it two standard deviation better than the average of the votes. And $\sim$ -2 for PTM in 15/20 of cases. In the other cases, and as explained before the gap between the performance of models decreases with less measurements and increases in some angles (phi = $14.5°$ and $55°$).

The Table XIII shows that the global mean and median of all the tested cases in the experiment, rank the accuracy of the reproduced images as PTM for the worst similarity to the original image, HSH as more accurate reproduction and DMD as the most accurate reproduction to the aspect of the surface. This conclusion match with results using the objective quality metrics (PSNR and SSIM).

TABLE IX
Z-SCORE FOR THE REPRODUCED IMAGES USING PTM, HSH, DMD AND 4 SAMPLING DENSITY (ALL, HALF, FIFTH AND SEVENTH) WITH THE ACQUIRED IMAGES IN DIFFERENT ANGLES.

Sampling	Angle	PTM	HSH	DMD
All (1): 650 position	$\theta : 180°, \phi : 14.5°$	-1,77	0,52	2,29
	$\theta : 180°, \phi : 28°$	-1,94	0,34	2,28
	$\theta : 180°, \phi : 41.5°$	-2,28	0,00	2,28
	$\theta : 180°, \phi : 55°$	-2,12	0,16	2,28
	$\theta : 88.61°, \phi : 41.5°$	-2,02	0,10	2,13
Half (1/2): 324 position	$\theta : 180°, \phi : 14.5°$	-2,28	0,34	1,94
	$\theta : 180°, \phi : 28°$	-2,02	0,26	2,28
	$\theta : 180°, \phi : 41.5°$	-2,02	0,10	2,13
	$\theta : 180°, \phi : 55°$	0,00	0,00	0,00
	$\theta : 88.61°, \phi : 41.5°$	-2,12	0,50	2,62
Fifth (1/5): 130 position	$\theta : 180°, \phi : 14.5°$	-2,13	0,10	2,02
	$\theta : 180°, \phi : 28°$	-2,12	0,16	2,28
	$\theta : 180°, \phi : 41.5°$	-2,02	0,10	2,13
	$\theta : 180°, \phi : 55°$	-2,65	0,62	2,03
	$\theta : 88.61°, \phi : 41.5°$	-2,13	0,10	2,02
Seventh (1/7): 93 position	$\theta : 180°, \phi : 14.5°$	-2,28	0,65	1,63
	$\theta : 180°, \phi : 28°$	-2,13	0,10	2,02
	$\theta : 180°, \phi : 41.5°$	-2,28	0,00	2,28
	$\theta : 180°, \phi : 55°$	0,00	0,00	0,00
	$\theta : 88.61°, \phi : 41.5°$	-1,16	0,12	1,30

The second part of the experiment was devoted to study the impact of the sampling density as explained in III-D1. Considering the number of times a reconstruction has been selected in Figure 8 computed using one surface and roughly the same result for the other four surfaces, we notice that

TABLE X
GLOBAL MEAN AND MEDIAN OF Z-SCORE COMPUTED OVER 5 REPRODUCED SURFACES' ASPECT IN 5 LIGHT DIRECTIONS

Method	Mean	Median
PTM	-1.87	-2.12
HSH	-0.02	-0.05
DMD	1.90	2.13

more measurements does not mean necessarily a better visual aspect. In the grazing angle ($\theta : 180°, \phi : 14.5°$) a higher sampling density where chosen: ALL= 30% of votes, HALF= 30%, FIFTH=30% as a higher quality representation of the original image. This ranking is changed for other angles (higher elevation) and less density of measurements is more accurate to the acquired image, 45% of votes were for the lower density (1/7) for the three angles and less then 15% for the highest sampling density and this is due to the extra perceived information that RTI provides to the image by integrating in computing the pixels' luminance for one angle, the luminance of the pixel in all lighting directions. And since the task of users is to choose the closer representation to the reference, the extra information disturbs their perceptual evaluation of the reconstructed images.

The results of mean z-score for the five angles and the five surfaces chosen for the experiment is presented in Table XII. For the different sampling density tested, the standard deviation to the mean is higher for a 1/7 of the measurements for the three angles ($\theta : 180°, \phi : 41.5°$),($\theta : 180°, \phi : 55°$),($\theta : 88.61°, \phi : 41.5°$) for all the surfaces. A full measurements density were preferred for a lower elevation ($\theta : 180°, \phi : 28°$),($\theta : 180°, \phi : 14.5°$) because in these angles, images are dark, so the perceptual evaluation is biased due to the limitation of the sensor which represent the values of pixel in only 1 byte. A future improvement of this investigation is to extend our acquisition to be able to build high dynamic range images. Computing the the global mean of the z-score in Table XIII for all the surfaces and the angles for each density ranks the quality of the reconstructed images using different sampling density respectively as: All, Half, Fifth and the seventh from the worst to the best perceived quality.

TABLE XI
GLOBAL MEAN AND MEDIAN OF Z-SCORE COMPUTED OVER 5 REPRODUCED SURFACES' ASPECT IN 5 LIGHT DIRECTIONS USING ALL, HALF, FIFTH AND SEVENTH OF MEASUREMENTS

Method	ALL	HALF	FIFTH	SEVENTH
Mean	-0.65	-0.43	0.50	0.58
Median	-0.77	-0.56	0.48	0.89

IV. CONCLUSION

The study presented in this paper aims to evaluate the quality of the reconstruction and relighted images using RTI stereo photo-metric images. The reconstruction models used: PTM, HSH, DMD with different sampling densities. The evaluation of the relighted images is done first with objective

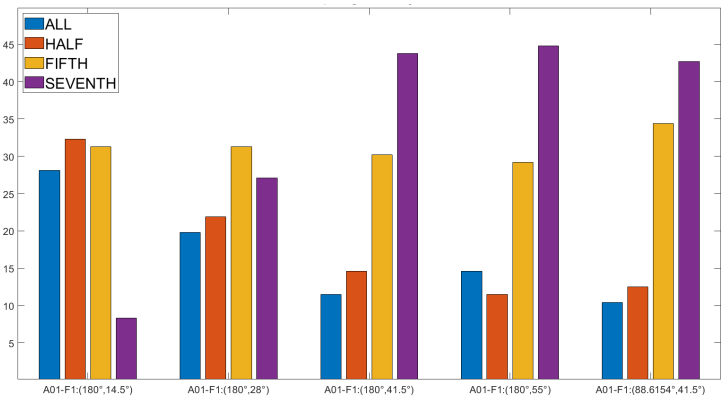

Fig. 8. Number of times a reproduction has been selected using four sampling density : All, Half, Fifth and a Seventh of the measurement using one of the five manufactured surfaces: A01

TABLE XII
Z-SCORE FOR THE REPRODUCED IMAGES USING DMD AND 4 SAMPLING DENSITY (ALL, HALF, FIFTH AND SEVENTH) WITH THE ACQUIRED IMAGES IN DIFFERENT ANGLES FOR THE FIVE SURFACES.

Surfaces	Angles	ALL	HALF	FIFTH	SEVEN
Surface 1:A01	$(180°, 14.5°)$	0,19	**0,41**	0,38	**0,97**
	$(180°, 28°)$	0,27	0,16	**0,32**	0,11
	$(180°, 41.5°)$	0,75	0,73	0,30	**1,19**
	$(180°, 55°)$	0,63	-1,04	0,22	**1,44**
	$(88.61°, 41.5°)$	0,95	-1,01	0,57	**1,38**
Surface 2: A04	$(180°, 14.5°)$	0,67	**0,17**	**0,35**	-1,19
	$(180°, 28°)$	0,68	**0,16**	**0,51**	0,34
	$(180°, 41.5°)$	0,91	-1,04	0,30	**1,66**
	$(180°, 55°)$	-1,06	0,52	0,67	**0,90**
	$(88.61°, 41.5°)$	0,68	0,89	0,67	**0,90**
Surface 3: A06	$(180°, 14.5°)$	0,49	**0,11**	**0,46**	-1,06
	$(180°, 28°)$	0,35	0,51	**0,75**	0,11
	$(180°, 41.5°)$	-1,00	0,92	0,73	**1,19**
	$(180°, 55°)$	-1,12	0,84	0,38	**1,57**
	$(88.61°, 41.5°)$	-1,00	0,79	0,51	**1,28**
Surface 4: A07	$(180°, 14.5°)$	0,38	**0,67**	0,06	-1,12
	$(180°, 28°)$	0,78	0,44	**0,95**	0,27
	$(180°, 41.5°)$	0,97	**0,38**	**0,52**	**0,84**
	$(180°, 55°)$	-1,19	0,69	0,38	**1,50**
	$(88.61°, 41.5°)$	**0,87**	0,66	0,66	**0,87**
Surface 5: A10	$(180°, 14.5°)$	0,05	0,49	0,34	0,77
	$(180°, 28°)$	0,83	0,16	0,71	0,28
	$(180°, 41.5°)$	-1,28	0,89	0,73	**1,44**
	$(180°, 55°)$	-1,37	0,58	0,38	**1,57**
	$(88.61°, 41.5°)$	-2,01	0,66	1,09	**1,70**

error metrics: PSNR and SSIM and second with psychometric experiment to involve the human subjective evaluation of surfaces as a reference for the perceptual evaluation of manufactured surfaces aspect. The subjective and objective evaluation of the surfaces' aspect shows that DMD outperforms PTM and HSH as a the most accurate model to approximate the perceptual aspect of a surface. The results shows also that the quality of the reconstruction using RTI-based images decreases with a high sampling density due to disturbance of the perceived quality with the amount of the not perceptual information to the human vision system.

TABLE XIII

	Values			
	Parameters level			
Material	-0.65	-0.43	0.50	0.58
Scale	-0.77	-0.56	0.48	0.89
Sampling density	-0.77	-0.56	0.48	0.89
Approximation model	-0.77	-0.56	0.48	0.89

REFERENCES

[1] T. Debrosse, M. Pillet, J. L. Maire, and N. Baudet, "Sensory perception of surfaces quality, Proceedings of KEER 2010.pdf," *INTERNATIONAL CONFERENCE ON KANSEI ENGINEERING AND EMOTION RESEARCH*, pp. 252–263, 2010.

[2] A. S. Guerra, "Sensory metrology in the environment of visual qulity control," Theses, Université de Savoie, Oct. 2008. [Online]. Available: https://tel.archives-ouvertes.fr/tel-00362743.

[3] J. D. Durou, "Shape from shading – Eclairages, réflexions et perspectives," Tech. Rep., 2007, p. 1 112. [Online]. Available: http : / / www . irit . fr / %5CtextbackslashtextasciitildeJean - Denis . Durou / PUBLICATIONS/hdr%5C_2007.pdf.

[4] T. Malzbender, D. Gelb, and H. Wolters, "Polynomial texture maps," *Proceedings of the ACM SIGGRAPH Conference on Computer Graphics*, vol. 2001, pp. 519–528, Jan. 2001. DOI: 10.1145/383259.383320.

[5] P. Gautron, J. Krivanek, S. N. Pattanaik, and K. Bouatouch, "A Novel Hemispherical Basis for Accurate and Efficient Rendering," *Eurographics Symposium on Rendering 2004*, p. 1 10, 2004.

[6] G. Pitard, G. Le Goic, A. Mansouri, H. Favreliere, S.-F. Désage, S. Samper, and M. Pillet, "Discrete Modal Decomposition: a new approach for the reflectance modeling and rendering of real surfaces," English, *Machine Vision and Applications*, p. 607 621, 2017, ISSN: 0932-8092. DOI: 10.1007/s00138-017-0856-0.

[7] Z. Wang, A. C. Bovik, H. R. Sheikh, and E. P. Simoncelli, "Image quality assessment: From error visibility to structural similarity," *Trans. Img. Proc.*, vol. 13, no. 4, pp. 600–612, Apr. 2004, ISSN: 1057-7149. DOI: 10.1109/TIP.2003.819861. [Online]. Available: http://dx.doi.org/10.1109/TIP.2003.819861.

[8] J. D. Durou, "Shape from shading – eclairages, ŕeflexions perspectives," 2007.

[9] L. Macdonald and S. Robson, "Polynomial texture mapping and 3d representations," *International Archives of the Photogrammetry, Remote Sensing and Spatial Information Sciences - ISPRS Archives*, vol. 38, pp. 422–427, Jan. 2010.

[10] S. H. Westin, J. R. Arvo, and K. E. Torrance, "Predicting reflectance functions from complex surfaces," *SIGGRAPH Comput. Graph.*, vol. 26, no. 2, pp. 255–264, Jul. 1992, ISSN: 0097-8930. DOI: 10.1145/142920.

134075. [Online]. Available: http://doi.acm.org/10.1145/142920.134075.

[11] P. Gautron, J. Krivanek, S. Pattanaik, and K. Bouatouch, "A novel hemispherical basis for accurate and efficient rendering," EGSR'04, pp. 321–330, 2004. DOI: 10.2312/EGWR/EGSR04/321-330. [Online]. Available: http://dx.doi.org/10.2312/EGWR/EGSR04/321-330.

[12] J. Kautz, P.-P. Sloan, and J. Snyder, "Fast, arbitrary brdf shading for low-frequency lighting using spherical harmonics," in *Proceedings of the 13th Eurographics Workshop on Rendering*, ser. EGRW '02, Pisa, Italy: Eurographics Association, 2002, pp. 291–296, ISBN: 1-58113-534-3. [Online]. Available: http://dl.acm.org/citation.cfm?id=581896.581934.

[13] R. Ramamoorthi and P. Hanrahan, "An efficient representation for irradiance environment maps," SIGGRAPH '01, pp. 497–500, 2001. DOI: 10.1145/383259.383317. [Online]. Available: http://doi.acm.org/10.1145/383259.383317.

[14] M. Ludwig and G. Meyer, "Environment Map Based Lighting for Reflectance Transformation Images," *2015 Digital Heritage*, vol. 1, pp. 385–388, 2015. DOI: 10.1109/digitalheritage.2015.7413909.

[15] P. A. Adragna, S. Samper, M. Pillet, and H. Favreliere, "Analysis of shape deviations of measured geometries with a modal basis," *Journal of Machine Engineering: Manufacturing Accuracy Increasing Problems–Optimization*, vol. 6, pp. 95–102, 2006.

[16] P. A. Adragna, S. Samper, F. Formosa, and M. Pillet, "Modal Tolerancing—Application to Gap and Flush Analyses," *Advances in Integrated Design and Manufacturing in Mechanical Engineering II*, p. 417 430, 2007.

[17] G. Julien, L. G. Gaëtan, F. Hugues, L. Yann, S. Serge, D. Laure, and G. Thomas, "Analyse multi-échelle des composants articulaires d'une prothèse de hanche par la méthode modale," *Congrès International Conception et Modélisation des Systèmes Mécaniques CMSM' 2011*, 2011.

[18] G. L. Goic, M. Bigerelle, S. Samper, H. Favreliere, and M. Pillet, "A benchmark of multiscale methods for tribological surfaces," 2013, p. 1 14.

[19] G. L. Goic, H. Favrelière, S. Samper, and F. Formosa, "Multi scale modal decomposition of primary form, waviness and roughness of surfaces," *Scanning*, vol. 33, pp. 332–341, 2011, ISSN: 1932-8745. DOI: 10.1002/sca.20253.

[20] T. Pottier, H. Louche, S. Samper, H. Favreliere, F. Toussaint, and P. Vacher, "A new filtering approach dedicated to heat sources computation from thermal field measurements," *PhotoMechanics Conference, Montpellier : France*, p. 1 4, 2013.

[21] T. Pottier, H. Louche, S. Samper, H. Favrelière, F. Toussaint, and P. Vacher, "Proposition of a modal filtering method to enhance heat source computation within heterogeneous thermomechanical problems," *International Journal of Engineering Science*, vol. 81, pp. 163–176, 2014, ISSN: 0020-7225. DOI: 10.1016/j.ijengsci.2014.04.010.

[22] G. Pitard, G. L. Goïc, H. Favrelière, S. Samper, S.-F. Desage, and M. Pillet, "Discrete Modal Decomposition for surface appearance modelling and rendering," in *Optical Measurement Systems for Industrial Inspection IX*, P. Lehmann, W. Osten, and A. A. G. Jr., Eds., International Society for Optics and Photonics, vol. 9525, SPIE, 2015, pp. 489–498. DOI: 10.1117/12.2184840. [Online]. Available: https://doi.org/10.1117/12.2184840.

[23] R. Pintus, T. Dulecha, A. Jaspe, A. Giachetti, I. Ciortan, and E. Gobbetti, "Objective and Subjective Evaluation of Virtual Relighting from Reflectance Transformation Imaging Data," R. Sablatnig and M. Wimmer, Eds., 2018, ISSN: 2312-6124. DOI: 10.2312/gch.20181344.

[24] C. Schuster, B. Zhang, R. Vaish, P. Gomes, J. Thomas, and J. Davis, "Rti compression for mobile devices," pp. 368–373, Nov. 2014. DOI: 10.1109/ICIMU.2014.7066661.

[25] F. Ponchio, M. Corsini, and R. Scopigno, "A compact representation of relightable images for the web," in *Proceedings of the 23rd International ACM Conference on 3D Web Technology*, ser. Web3D '18, Poznań, Poland: ACM, 2018, 1:1–1:10, ISBN: 978-1-4503-5800-2. DOI: 10.1145/3208806.3208820. [Online]. Available: http://doi.acm.org/10.1145/3208806.3208820.

[26] K. V. Ngo, J. J. Storvik, C. A. Dokkeberg, I. Farup, and M. Pedersen, "QuickEval: a web application for psychometric scaling experiments," vol. 9396, M.-C. Larabi and S. Triantaphillidou, Eds., pp. 212–224, 2015. DOI: 10.1117/12.2077548. [Online]. Available: https://doi.org/10.1117/12.2077548.

[27] P. G. ENGELDRUM, *Psychometric scaling: a toolkit for imaging systems development*. Winchester, Mass, Imcotek Press., 2000.